OPTIMAL CONTROL APPLICATIONS AND METHODS
Optim. Control Appl. Meth. 2013; **34**:202–215
Published online 14 February 2012 in Wiley Online Library (wileyonlinelibrary.com). DOI: 10.1002/oca.2017

A time-varying coefficient-based manipulability-maximizing scheme for motion control of redundant robots subject to varying joint-velocity limits

Yunong Zhang*,†, Jun Li and Zhijun Zhang

School of Information Science and Technology, Sun Yat-sen University, Guangzhou 510006, China

SUMMARY

A time-varying coefficient-based manipulability-maximizing (TVCMM) scheme subject to varying joint-velocity limits (VJVL) is proposed and investigated in this paper for the optimal motion control of redundant robot manipulators (where a planar robot manipulator is specifically considered). In order to improve the manipulability during the end-effector task execution, a manipulability-maximizing index is considered into the scheme formulation. Besides, for the remedy of the nonzero initial/final joint-velocity problem, a time-varying coefficient is introduced and incorporated in the scheme, which is further reformulated as a quadratic program (QP) subject to equality and bound constraints. For guaranteeing the physical realizability of such a scheme, an efficient linear variational inequality-based (LVI-based) numerical algorithm is employed to solve such a QP, and an experiment based on a 6-DOF manipulator is presented, of which the redundancy is on the horizontal plane. Simulative and experimental results validate the physical realization, effectiveness, and accuracy of the proposed QP-based manipulability-maximizing scheme. Copyright © 2012 John Wiley & Sons, Ltd.

Received 20 May 2011; Revised 16 September 2011; Accepted 10 December 2011

KEY WORDS: optimal motion control; manipulability maximization; quadratic program (QP); LVI-based numerical algorithm; time-varying coefficient; varying joint-velocity limits (VJVL); redundancy resolution

1. INTRODUCTION

The issue of optimal motion control in robotics is becoming a more and more appealing topic as robots are widely applied in scientific research, in military, and civilian areas, of which the operating environment is much more complicated than in the past [1–4]. Redundant manipulators can achieve subtasks, such as obstacle avoidance [5], repetitive motion planning [6], joint limits and singularity avoidance [7–10], or optimization of various performance criteria [11], because they have more DOF than required to perform a given end-effector primary task [12]. A fundamental issue in controlling such redundant manipulators is to design suitable redundancy-resolution approaches [11, 12]. The conventional solution to such a redundancy-resolution problem is the pseudoinverse-based formulation [7]. For instance, in [8], Soylu *et al.* presented a pseudoinverse-based redundancy-resolution scheme for a 6-DOF underwater vehicle-manipulator system, which can take multi-objectives into consideration as the secondary task, such as avoiding the manipulator's joint limits, avoiding singularities, and preventing high joint velocities. In recent years, to avoid online matrix inversion and achieve higher computation efficiency, many efforts have been made to find the solution of the redundancy-resolution problem via optimization techniques [12].

*Correspondence to: Yunong Zhang, School of Information Science and Technology, Sun Yat-sen University, Guangzhou 510006, China.

†E-mail: zhynong@mail.sysu.edu.cn; jallonzyn@sina.com

Generally speaking, such techniques can reformulate different schemes as a unified quadratic program (QP) which is subject to equality, inequality, and bound constraints. Because the QP is equivalent to a linear variational inequality (LVI) problem, it can be solved through many methods and techniques efficiently, for example, LVI-based numerical algorithms [13] and/or recurrent neural networks [6, 12].

A singularity problem can refer to a situation when the manipulator's Jacobian matrix is ill-conditioned and loses rank at a kinematic singular point [14] and can refer to when nearby a singular point of the kinematic mapping, joint velocities, accelerations, and torques may become too large when the end-effector moves in certain directions [15]. To keep the manipulator away from singular points, Yoshikawa first introduced, with explicit expression, the kinematic manipulability as a well-established tool in the design or motion control of redundant robot manipulators which can reflect the manipulator's ability to affect the end-effector's velocities and accelerations [16] . In that paper, Yoshikawa proposed a pseudoinverse-based algorithm for singularity avoidance of redundant manipulators by maximizing the manipulability measure, where the simulation example based on a planar three-link redundant robot was given. In [9], Mitsi *et al.* discussed the problem of finding the optimum base location and configurations of the manipulator, which was realized by maximizing the manipulability of the robot. In addition, the optimization problem was solved by using a hybrid genetic algorithm. In [17], Huang *et al.* proposed a method for a finger-arm robot to complete an impedance control by regulating the finger's manipulability and found that the impedance performance at the fingertip is greatly determined by the manipulability of the finger. In [10], by introducing a scalar function which was composed of a task-oriented manipulability measure and a joint limit measure as an object of optimization, Jun *et al.* focused on enhancing the functionality of a tele-operated underwater manipulator. In that paper, sequential quadratic programming was firstly used to find the optimal configuration for the manipulator. Then, a pseudoinverse-based approach was adopted for motion planning. Different from the above, this paper adopts the QP-technique to solve the redundancy-resolution problem of redundant robot manipulators (note that a 6-DOF planar robot manipulator is specifically considered) and simultaneously maximizes the kinematic manipulability. This is realized by utilizing the redundant DOF of the robot to adjust its configuration in joint space during the end-effector task execution.

Among those existing methods and techniques, the physical constraints, such as the joint-velocity limits, are usually considered to be constant. This, however, may not be applicable to some kinds of manipulators, such as the robot manipulators with push-rod-type joints (also called push-rod-joint manipulators), of which the joint-velocity limits change with the end-effector and joints' movement (i.e., joint-velocity limits are functions of joint angles). In this paper, a time-varying coefficient-based manipulability-maximizing (TVCMM) scheme subject to varying joint-velocity limits (VJVL) is proposed and analyzed. Furthermore, such a scheme is implemented on a 6-DOF push-rod-joint manipulator.

The remainder of this paper is organized as follows. In Section 2, the hardware system of a planar 6-DOF redundant robot manipulator is presented and analyzed, of which the joints are driven by a servo motor (for the first joint) and five stepper motors (for Joints 2–6). In Section 3, a novel TVCMM scheme subject to VJVL is proposed and then reformulated in the unified form of a QP. What is more, an LVI-based numerical algorithm is developed and employed to solve such a QP problem. In Section 4, both the computer simulations and the hardware experiment based on the 6-DOF robot manipulator verify the physical realizability and effectiveness of such a TVCMM scheme (including the corresponding LVI-based numerical algorithm). In addition, the experimental results and the positioning-error analysis validate the accuracy of such an optimal-control scheme. Section 5 concludes this paper with final remarks. Before ending this section, it is worth pointing out here that this paper has the following main contributions.

(i) A planar 6-DOF manipulator hardware system is presented, of which the first joint is of rotary type and driven by a servo motor, whereas the other five joints, being of push-rod type, are driven by stepper motors. In addition, the joint-velocity limits are related to the joint-angle states. That is to say, they are varying with the end-effector and joints' movement.

DOI: 10.1002/oca

(ii) The issue of maximizing kinematic manipulability (by adjust configuration in joint space) during the end-effector task execution is investigated and analyzed theoretically. This paper, for the first time, formulates the time-varying coefficient-based manipulability-maximizing problem into a unified quadratic programm and solves the resultant QP by employing an LVI-based numerical algorithm. In addition, the joint physical limits are considered into such a QP scheme as a combined bound constraint.

(iii) A nonzero initial/final joint-velocity phenomenon,which can be solved elegantly by designing a time-varying coefficient in the manipulability-maximizing scheme instead of using a constant coefficient, is discussed and analyzed.

(iv) An LVI-based numerical algorithm based on the QP-to-LVI conversion is presented to solve the time-varying QP problem constrained by the aforementioned varying joint-velocity limits.

(v) As synthesized by the proposed TVCMM scheme, a user-specified end-effector task (i.e., the letter "R" writing) is performed on the presented planar 6-DOF manipulator. Comparative results based on computer simulations of the TVCMM scheme and the minimum velocity norm (MVN) scheme, together with experiment-result analysis, demonstrate the physical realizability, effectiveness, and superiority of such a TVCMM scheme. Furthermore, for validating the effectiveness of the time-varying coefficient of the manipulability-maximizing index, the comparisons are made with the simulation results using a constant–coefficient index. In addition, the positioning-error analysis validates the accuracy of such an optimal-control scheme.

2. HARDWARE SYSTEM DESCRIPTION

Mechanisms of the push-rod type are widely applied in various industrial robot systems, in view of their remarkable ability of providing powerful force. To conveniently illustrate the TVCMM scheme for optimal motion control and its physical applicability, we introduce a planar 6-DOF push-rod-joint manipulator, shown in Figure 1. The left photo of Figure 1 shows the manipulator hardware system in the laboratory. The corresponding top-view of its computer-aided design (CAD) model is presented in the right image of Figure 1. Joint 1, being a rotary-type joint, employs a servo motor to provide wide operating range. Joints 2–6, being of push-rod type, are driven by stepper motors. The ith joint ($i = 2, 3, \cdots, 6$) is shown in the left photo of Figure 2, which can be viewed as a triangle depicted in the right image of Figure 2. In this figure, the three edges (denoted by thick dashed lines) of the triangle are a_i, b_i, and c_i ($i = 2, 3, \cdots, 6$), respectively. The geometric parameters are shown in Table I, where l_i denotes the length of the ith link, whereas θ_i^+ and θ_i^- denote the upper and lower limits of the ith joint-angle θ_i, respectively, for $i = 1, 2, \cdots, 6$.

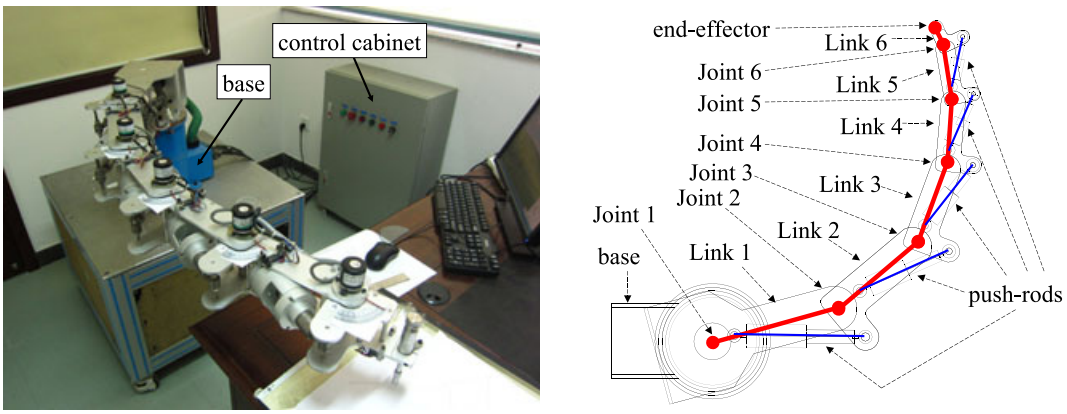

Figure 1. Hardware system in the lab and its simplified CAD model of the 6-DOF redundant robot manipulator with push rod-type joints.

DOI: 10.1002/oca

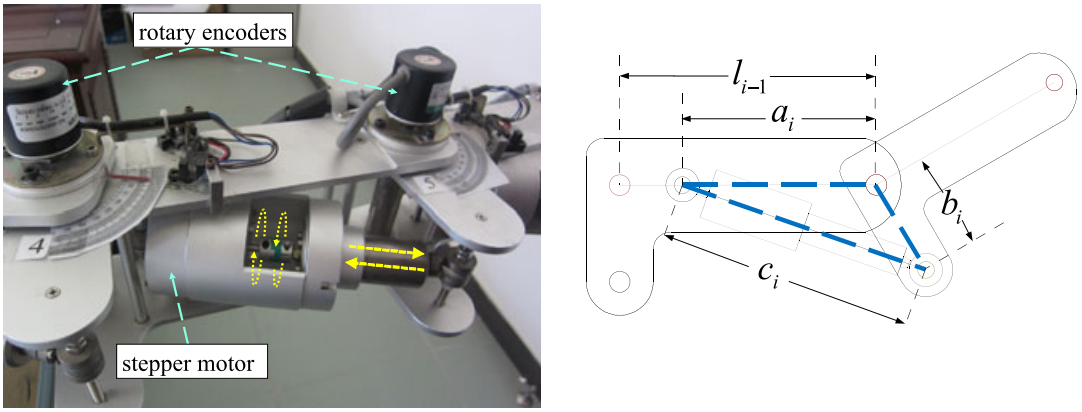

Figure 2. The local joint-structure of the 6-DOF redundant robot manipulator.

Table I. Geometric parameters of the 6-DOF push-rod-joint robot manipulator.

	$i=1$	$i=2$	$i=3$	$i=4$	$i=5$	$i=6$
a_i (m)	—	0.250	0.250	0.190	0.185	0.174
b_i (m)	—	0.080	0.080	0.080	0.080	0.080
l_i (m)	0.301	0.290	0.230	0.225	0.214	0.103
θ_i^+ (rad)	1.431	0.785	0.611	0.576	0.559	0.445
θ_i^- (rad)	−1.536	0.052	0.026	0.066	0.017	0.009

Furthermore, corresponding to Figure 1, the upper and lower velocity limits of Joint 1 are $\dot{\theta}_1^{\pm} = \pm 25\pi/24$ rad/s, according to the derivation based on the motor parameters. Different from Joint 1, joint-velocity $\dot{\theta}_i (i = 2, 3, \cdots, 6)$ and the rotation rate σ_i of the stepper motor have the following relationship according to the joint-structure and stepper motor parameters:

$$\dot{\theta}_i = \frac{s_i \sigma_i \sqrt{a_i^2 + b_i^2 + 2a_i b_i \sin\theta_i}}{a_i b_i \cos\theta_i}, \text{ with } i = 2, 3, \cdots, 6 \tag{1}$$

where s_i denotes the elongation rate of the ith push-rod (i.e., the elongation length when the motor moves a full turn). For this manipulator hardware system, $s_i = 2.5 \times 10^{-3}$ m/rot, $i = 2, 3, \cdots, 6$. Now, substituting the limits of σ_i into (1), the ith joint-velocity limits $\dot{\theta}_i^{\pm}(\theta_i)$, in $\dot{\theta}_i^-(\theta_i) \leqslant \dot{\theta}_i \leqslant \dot{\theta}_i^+(\theta_i)$, can be obtained as

$$\dot{\theta}_i^{\pm}(\theta_i) = \frac{s_i \sigma_i^{\pm} \sqrt{a_i^2 + b_i^2 + 2a_i b_i \sin\theta_i}}{a_i b_i \cos\theta_i} \tag{2}$$

where σ_i^+ and σ_i^- denote, respectively, the positive and negative rotation-rate limits of the ith stepper motor, and in the robot system, $\sigma_i^+ = -\sigma_i^- = 10$ rot/s. It can be seen from (2) that joint-velocity limits $\dot{\theta}_i^{\pm}$ are not constant but varying with joint-angle θ_i [i.e., varying joint-velocity limits (VJVL)].

Besides the above mentioned manipulator, the robot-arm system consists of a personal computer and a control cabinet as the main processing and control modules. The computer is equipped with a Pentium E5300 2.6 GHz CPU, a 4 GB memory, and runs within the Windows XP Professional operating system environment. The computer sends instructions (about the computed $\dot{\theta}$ and θ) to the manipulator motion-control module [i.e., a six-axis control card of peripheral component interconnect (PCI)] to operate the manipulator.

DOI: 10.1002/oca

3. MANIPULABILITY MAXIMIZATION WITH TIME-VARYING COEFFICIENT

This section discusses the TVCMM scheme. Firstly, this scheme, with joint physical limits considered, is proposed and reformulated into a QP. Secondly, an LVI-based numerical algorithm is presented to solve effectively such a time-varying QP problem which is subject to equality and bound constraints. On the basis of the solutions (i.e., the computed $\dot{\theta}$ and θ) of the proposed optimal-control scheme, the planar 6-DOF redundant robot manipulator can fulfill the user-specified end-effector task. It is worth mentioning that, during the task execution, the manipulability can keep maximizing, which means that the manipulator maintains its optimality and is away from singular points.

3.1. Nonzero initial/final joint-velocity problem

The relation between the end-effector position-and-orientation vector $r(t) \in R^m$ in the Cartesian space and the joint-angle vector $\theta(t) \in R^n$ in the joint space can be described as $r = f(\theta)$ and $\dot{r} = J(\theta)\dot{\theta}$, where $f(\cdot)$ is a nonlinear mapping from R^n to R^m. $\dot{r} \in R^m$ is the time-derivative of r (i.e., the end-effector velocity, or termed as the Cartesian velocity), whereas $J(\theta) = \partial f(\theta)/\partial\theta \in R^{m\times n}$ denotes the Jacobian matrix. Note that $r(t)$, $\theta(t)$, and $J(\theta)$ are sometimes written as r, θ, and J, respectively, for presentation convenience. In this paper, $m = 2$ because we consider only the end-effector position, and $n = 6$ in view of the manipulator having 6 DOF.

During the past decades, the kinematic manipulability has been used in the optimal control of robot manipulators [8–10, 16–20], and the quantitative measure of manipulability at configuration θ can be given as $w = \det(JJ^{\mathrm{T}})$. Here, "det(·)" denotes the determinant of a matrix, and superscript $^{\mathrm{T}}$ denotes the transpose of a matrix or vector. Note that w is quite helpful for the detailed evaluation of the manipulation ability of a robotic mechanism; for example, w could give an overall measure of the directional uniformity of the ellipsoid and the upper bound of the velocity with which the end-effector could be moved in any directions [18]. Therefore, it could be used as an important reference factor on the configuration adjustment of redundant manipulators via self-motion. Inspired by the gradient method in optimization [21–23], for maximizing the manipulability w, we can design

$$\dot{\theta} = p\frac{\partial \det(JJ^{\mathrm{T}})}{\partial\theta} \tag{3}$$

where, conventionally speaking, $p \in R$ is a positive design parameter. In the pseudoinverse-based formulation,

$$\dot{\theta} = \dot{\theta}_{\mathrm{p}} + \dot{\theta}_{\mathrm{h}} = J^{\dagger}\dot{r} + (I - J^{\dagger}J)\,p\frac{\partial \det(JJ^{\mathrm{T}})}{\partial\theta}$$

where I denotes an appropriately dimensioned identity matrix and $J^{\dagger} \in R^{n\times m}$ denotes the pseudoinverse of J. Projection matrix $(I - J^{\dagger}J) \in R^{n\times n}$ is utilized to project $p(\partial \det(JJ^{\mathrm{T}})/\partial\theta)$ onto the null-space of J to keep the manipulator away from singularities without having an affect on the end-effector task execution [24–26]. Here, $\dot{\theta}_{\mathrm{p}} = J^{\dagger}\dot{r}$ denotes the particular solution (i.e., the minimum Euclidean-norm solution) to $\dot{r} = J(\theta)\dot{\theta}$, and $\dot{\theta}_{\mathrm{h}} = (I - J^{\dagger}J)\,p(\partial \det(JJ^{\mathrm{T}})/\partial\theta)$ denotes the homogeneous solution which is referred to as the self-motion of the manipulator and can keep the manipulator away from the singularities by maximizing the manipulability w.

It is worth noting that the particular solution $\dot{\theta}_{\mathrm{p}} = J^{\dagger}\dot{r}$ generates zero initial and final joint velocities, when $\dot{r}(t)$ starts from a zero initial value and ends with a zero final value. However, the homogeneous solution $\dot{\theta}_{\mathrm{h}} = (I - J^{\dagger}J)\,p(\partial \det(JJ^{\mathrm{T}})/\partial\theta)$ would lead to nonzero initial and final joint velocities because the gradient, $\partial \det(JJ^{\mathrm{T}})/\partial\theta$, may not equal zero at the initial and final time instants, which is usually the case. As a result, $\dot{\theta} = \dot{\theta}_{\mathrm{p}} + \dot{\theta}_{\mathrm{h}}$ can cause a nonzero initial/final joint-velocity phenomenon. The phenomenon may induce the problem that large (or even infinitely large) joint-accelerations arise at the beginning of the task duration. It is not suitable for engineering application and can even cause damage to the hardware system.

DOI: 10.1002/oca

For the remedy of the nonzero initial/final joint-velocity problem, this paper proposes using a time-varying coefficient $p(t)$ instead of a constant coefficient p. We simply design $p(t) = p_1 \sin(\pi t/T)$, where constant parameter $p_1 \in R$ is used to scale the maximum magnitude of coefficient $p(t)$, and T is the task duration. It is worth mentioning that time-varying coefficient $p(t)$ is nonnegative, continuous, and differentiable, in addition to $p(0) = p(T) = 0$.

3.2. Scheme formulation

To improve the manipulability of the robot manipulator and fulfill the desired end-effector task, according to (3) and $p(t) = p_1 \sin(\pi t/T)$, we define the following performance index to be minimized: $E(t) = \|\dot{\theta}(t) - p(t)q(\theta(t))\|_2^2/2$, or $E = \|\dot{\theta} - pq\|_2^2/2$ in short, where $\|\cdot\|_2$ denotes the two-norm of a vector and $q = q(\theta) = \partial \det(JJ^{\mathrm{T}})/\partial\theta \in R^n$. Note that, as the robot's end-effector task requirement $J\dot{\theta} = \dot{r}$ should be considered into the scheme formulation, it is better to minimize E rather than force $\dot{\theta} = pq$ [i.e., (3)] directly. By minimizing E, the manipulability of the manipulator can be maximized during the task execution. Besides, E can be expanded as

$$\begin{aligned} E &= \|\dot{\theta} - pq\|_2^2/2 = (\dot{\theta} - pq)^{\mathrm{T}}(\dot{\theta} - pq)/2 \\ &= \left(\dot{\theta}^{\mathrm{T}}\dot{\theta} - \dot{\theta}^{\mathrm{T}}pq - pq^{\mathrm{T}}\dot{\theta} + p^2q^{\mathrm{T}}q\right)/2 \\ &= \dot{\theta}^{\mathrm{T}}\dot{\theta}/2 - pq^{\mathrm{T}}\dot{\theta} + p^2q^{\mathrm{T}}q/2 \end{aligned} \tag{4}$$

Via (4), minimizing E is equivalent to minimizing $\dot{\theta}^{\mathrm{T}}\dot{\theta}/2 - pq^{\mathrm{T}}\dot{\theta}$ in the velocity-level redundancy-resolution scheme, and the TVCMM scheme, subject to varying joint-velocity limits [i.e., (2)], is thus proposed as

$$\begin{aligned} &\text{minimize} && \dot{\theta}^{\mathrm{T}}\dot{\theta}/2 - p(t)q^{\mathrm{T}}\dot{\theta} && (5)\\ &\text{subject to} && J\dot{\theta} = \dot{r} + K(r - f(\theta)) && (6)\\ & && \theta^- \leqslant \theta \leqslant \theta^+ && (7)\\ & && \dot{\theta}^-(\theta) \leqslant \dot{\theta} \leqslant \dot{\theta}^+(\theta) && (8)\\ & && \text{with } q = \frac{\partial \det(JJ^{\mathrm{T}})}{\partial\theta} \end{aligned}$$

where θ^+ and θ^- denote, respectively, the upper and lower limits of joint-angle vector θ; and, resulting from $\dot{\theta}_1^{\pm} = \pm 25\pi/24$ and (2), $\dot{\theta}^+(\theta)$ and $\dot{\theta}^-(\theta)$ denote, respectively, the upper and lower limits of joint-velocity vector $\dot{\theta}$, which vary with θ. To achieve higher precision and robustness of end-effector positioning, it is necessary to introduce a feedback of the Cartesian position error into the redundancy-resolution equation, that is, $J\dot{\theta} = \dot{r} + K(r - f(\theta))$, where K is a positive-definite symmetric (typically diagonal) $m \times m$ feedback-gain matrix (in the ensuing simulations and experiment, $K = 8I$ with $I \in R^{m\times m}$ denoting the identity matrix). In addition, with $i = 1, 2, \cdots, 6$, the ith element of q can be given mathematically [16] as

$$\begin{aligned} q_i = \frac{\partial \det(JJ^{\mathrm{T}})}{\partial\theta_i} &= \det(JJ^{\mathrm{T}})\,\mathrm{trace}\left((JJ^{\mathrm{T}})^{-1}\frac{\partial(JJ^{\mathrm{T}})}{\partial\theta_i}\right) \\ &= \det(JJ^{\mathrm{T}})\,\mathrm{trace}\left((JJ^{\mathrm{T}})^{-1}\left(\frac{\partial J}{\partial\theta_i}J^{\mathrm{T}} + J\left(\frac{\partial J}{\partial\theta_i}\right)^{\mathrm{T}}\right)\right) \end{aligned}$$

Here, trace$(\cdot)$ denotes the trace of a matrix argument.

Furthermore, as the redundancy is resolved at the joint-velocity level (i.e., in terms of $\dot{\theta}$), joint-angle limit constraint (7) has been converted into the following expression about $\dot{\theta}$ [6]:

$$\kappa(\theta^- - \theta) \leqslant \dot{\theta} \leqslant \kappa(\theta^+ - \theta) \tag{9}$$

where $\kappa > 0 \in R$ is used to scale the feasible region of joint-velocity $\dot{\theta}$. Note that, in the presented planar 6-DOF manipulator of this paper, the safety devices are used. If a joint of the manipulator

DOI: 10.1002/oca

approaches or reaches its physical limit, the joint would be locked by the physical safety device throughout the task duration, which would lead to the failure of the end-effector task execution. It is thus necessary to leave some "safety region" to the joint physical limits $\theta^{\pm}$. So, (9) can be further improved into the following expression:

$$\kappa\left((\theta^{-}+\vartheta)-\theta\right) \leqslant \dot{\theta} \leqslant \kappa\left((\theta^{+}-\vartheta)-\theta\right)$$

where ϑ is a constant vector used to scale the safety region, with each element ϑ_i $(i = 1, 2, \cdots, 6)$ set to be 0.0349 rad (i.e., 2 degrees) in the simulations and the experiment of this paper.

Therefore, the physically-constrained TVCMM scheme can be formulated as a quadratic program:

$$\begin{aligned} &\text{minimize} && x^{\mathrm{T}}Wx/2 + \varsigma^{\mathrm{T}}x && (10)\\ &\text{subject to} && Jx = d && (11)\\ & && \zeta^{-} \leqslant x \leqslant \zeta^{+} && (12)\\ & && \text{with } x = \dot{\theta},\ W = I,\ \varsigma = -p(t)q,\ d = \dot{r} + K(r - f(\theta)) \end{aligned}$$

where the ith elements of ζ^{-} and ζ^{+} (with $i = 1, 2, \cdots, 6$) are

$$\zeta_i^{-} = \max\{\kappa\left((\theta_i^{-}+\vartheta_i)-\theta_i\right), \dot{\theta}_i^{-}(\theta_i)\},\ \zeta_i^{+} = \min\{\kappa\left((\theta_i^{+}-\vartheta_i)-\theta_i\right), \dot{\theta}_i^{+}(\theta_i)\}$$

Note that the performance index, (10), is for manipulability-maximizing purposes; the equality constraint, (11), expresses the linear relation between the joint-velocity vector and the desired Cartesian velocity of the end-effector, with position-error feedback $K(r - f(\theta))$ included; to keep all joint variables within their mechanical ranges, it is straightforward and concise to use bound constraint (12). It is also worth noting that, besides the end-effector path-tracking primary task (11), in this paper, the additionally considered secondary tasks for redundancy-resolution are the manipulability maximization and the avoidance of joint physical limits, especially avoiding the varying joint-velocity limits depicted in (2).

3.3. *Quadratic program solver*

In view of the duality theory and the authors' previous work [26], QP problems (10)–(12) can be converted to an LVI. That is, to find a primal-dual vector $u^* \in \Omega = \{u \in R^{n+m} | u^{-} \leqslant u \leqslant u^{+}\} \subset R^{n+m}$ such that

$$(u - u^*)^{\mathrm{T}}(Mu^* + g) \geqslant 0,\ \forall u \in \Omega \tag{13}$$

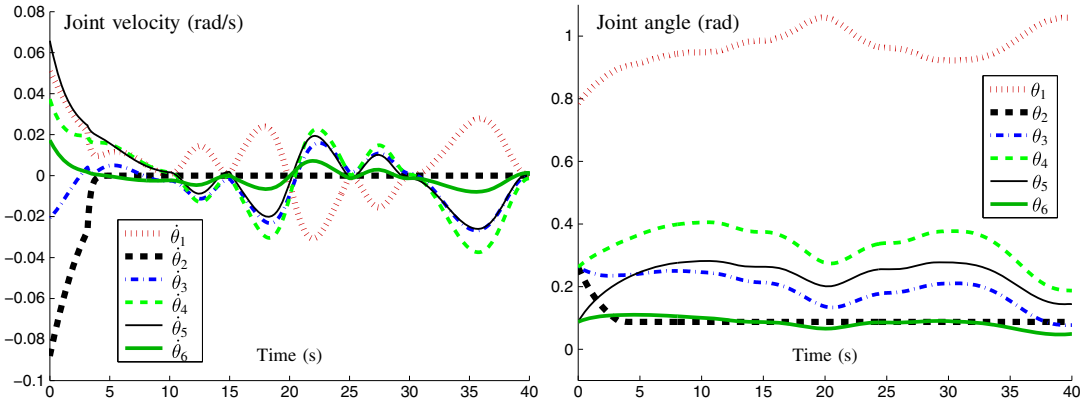

(a) $\dot{\theta}$-profiles with $p(t) = 1$ (b) θ-profiles with $p(t) = 1$

Figure 3. Joint-velocity and joint-angle profiles of the 6-DOF manipulator synthesized by the manipulability-maximizing scheme with a constant coefficient $p(t) = 1$. (a) $\dot{\theta}$-profiles with $p(t) = 1$ and (b) θ-profiles with $p(t) = 1$.

DOI: 10.1002/oca

where

$$u = \begin{bmatrix} x \\ y \end{bmatrix} \in R^{n+m},\ u^+ = \begin{bmatrix} \zeta^+ \\ \varpi 1_{\mathrm{v}} \end{bmatrix} \in R^{n+m},\ u^- = \begin{bmatrix} \zeta^- \\ -\varpi 1_{\mathrm{v}} \end{bmatrix} \in R^{n+m}$$

$$M = \begin{bmatrix} W & -J^{\mathrm{T}} \\ J & 0 \end{bmatrix} \in R^{(n+m)\times(n+m)},\ g = \begin{bmatrix} \varsigma \\ -d \end{bmatrix} \in R^{n+m},\ 1_{\mathrm{v}} := [1, \cdots, 1]^{\mathrm{T}} \in R^m$$

Here, $y \in R^m$ is the dual decision variable vector defined for equality constraint (11), and $\varpi \gg 0 \in R$ is defined as a sufficiently large number (e.g., $\varpi = 10^6$) to replace $+\infty$ numerically. It is further known that solving LVI (13) is equivalent to solving the following piecewise linear equation:

$$P_\Omega(u - (Mu + g)) - u = 0 \tag{14}$$

where $P_\Omega(\cdot) : R^{n+m} \to \Omega$ is a projection operator, with the ith element of $P_\Omega(z)$ defined as

$$\begin{cases} u_i^- & \text{if } z_i < u_i^-, \\ z_i & \text{if } u_i^- \leqslant z_i \leqslant u_i^+,\ \forall i \in \{1, 2, \cdots, n+m\}. \\ u_i^+ & \text{if } z_i > u_i^+, \end{cases}$$

To solve (14) [as well as LVI (13) and QP (10)–(12)], let us first define the solution set, $\Omega^* = \{u^* | u^* \text{ is a solution of (14)}\}$, and a continuous error function, $e(u) = u - P_\Omega(u - (Mu + g))$.

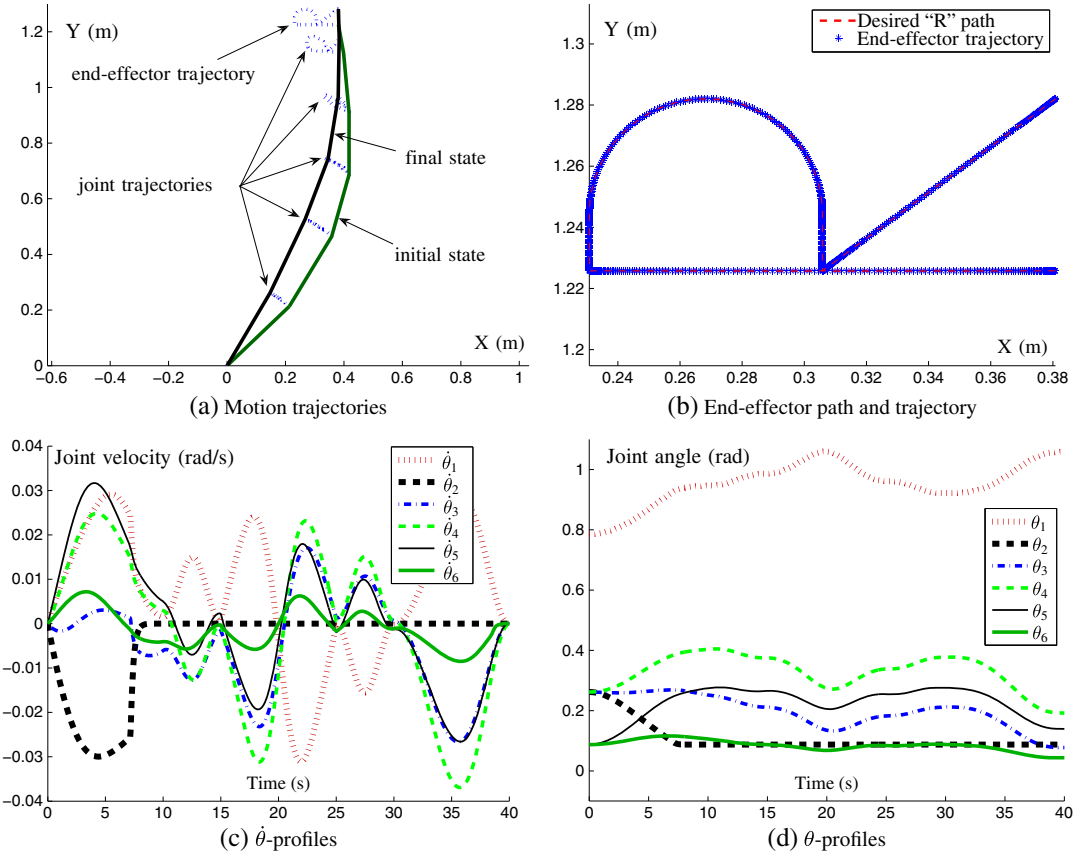

(a) Motion trajectories (b) End-effector path and trajectory

(c) $\dot{\theta}$-profiles (d) θ-profiles

Figure 4. The end-effector of the planar 6-DOF manipulator tracks the "R" path, which is synthesized by the time-varying coefficient-based manipulability-maximizing scheme (i.e., $p(t) = 2\sin(\pi t/T)$). (a) Motion trajectories, (b) end-effector path and trajectory, (c) $\dot{\theta}$-profiles, and (d) θ-profiles.

DOI: 10.1002/oca

According to [13], LVI-converted piecewise linear equation (14) can be solved with the following numerical algorithm. Given the initial value of primal-dual decision variable vector $u^0 \in R^{n+m}$ for iteration number $k = 0, 1, 2, 3, \cdots$, if $u^k \notin \Omega^*$, the numerical iterative formula for u^{k+1} is

$$u^{k+1} = u^k - \frac{\|e(u^k)\|_2^2 \varphi(u^k)}{\|\varphi(u^k)\|_2^2} \tag{15}$$

where $\varphi(u^k) = (M^{\mathrm{T}} + I)e(u^k)$. In addition, as generalized from Theorems 1–3 of [13], the sequence $\{u^k\}$ generated by LVI-based numerical algorithm (15) globally linearly converges to solution u^*, of which the first n elements constitute the optimal solution x^* (i.e., the computed $\dot{\theta}$) to QP (10)–(12). The QP problem and the original TVCMM scheme are thus solved.

4. SIMULATIVE AND EXPERIMENTAL VERIFICATION

In order to test the TVCMM scheme, computer simulations and an experiment are performed by using the planar 6-DOF robot manipulator to track an "R" path in the two-dimensional horizontal work-plane (i.e., the motion plane of the whole robot is parallel to the X–Y plane). For the "R" path to be tracked, the character height is set to 0.15 m, the task duration $T = 40$ s, and the initial joint state $\theta(0) = [\pi/4, \pi/12, \pi/12, \pi/12, \pi/36, \pi/36]^{\mathrm{T}}$ in radians. In addition, design parameters are $p_1 = 2$ and $\kappa = 4$. Furthermore, throughout this section, the error tolerance $\|e(u^k)\|_2 \leqslant 1.0 \times 10^{-6}$ is checked and guaranteed to assume $u^k \in \Omega^*$ in the QP-solving numerical algorithm (15), which is very accurate for the simulations and the experiment .

4.1. Computer simulation verification

Firstly, for comparison, the simulation results synthesized by the constant coefficient-based manipulability-maximizing scheme with $p(t) = 1$ are demonstrated, which are shown in Figure 3. Specifically, Figure 3(a) shows the joint-velocity profiles when the end-effector of the planar 6-DOF redundant robot manipulator tracks the "R" path. As seen from the figure, initial joint-velocity $\dot{\theta}(0) \neq 0$. That is to say, an abrupt change of joint-velocity happens at the beginning of the task execution, which is undesirable for engineering applications. The reason is similar to that given in Section 3.1, the homogeneous solution is nonzero at the beginning of the task. Besides, Figure 3(b) shows the corresponding joint-angle profiles.

Secondly, synthesized by the time-varying coefficient-based manipulability-maximizing scheme with $p(t) = 2\sin(\pi t/T)$, the simulation results are generated and shown mainly in Figure 4. Specifically, Figure 4(a) illustrates the simulated planar 6-DOF manipulator, of which the end-effector tracks the "R" path. As seen from the figure, the end-effector trajectory is very close to the desired path, which validates that the task is completed well. In addition, Figure 4(b) illustrates

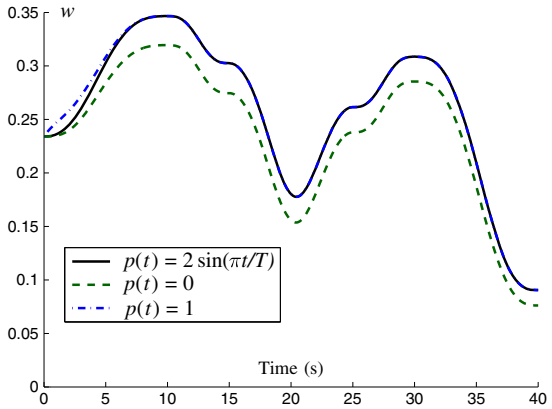

Figure 5. Comparison of the manipulability index $w = \det(JJ^{\mathrm{T}})$ synthesized by schemes with $p(t) = 2\sin(\pi t/T)$, $p(t) = 0$ (i.e., an MVN scheme), and $p(t) = 1$.

DOI: 10.1002/oca

the desired path and the end-effector trajectory, which coincide well with each other. Furthermore, Figure 4(c and d) show, respectively, the corresponding joint-velocity and joint-angle profiles of the planar 6-DOF manipulator when its end-effector tracks the "R" path, as synthesized by the proposed TVCMM scheme. Comparing Figure 4(c and d) with Figure 3, we can observe that all joint velocities now start from zero continuously and smoothly, and also return to zero. That is to say, by exploiting the time-varying coefficient $p(t) = 2\sin(\pi t/T)$, the nonzero initial/final joint-velocity phenomenon can be remedied well.

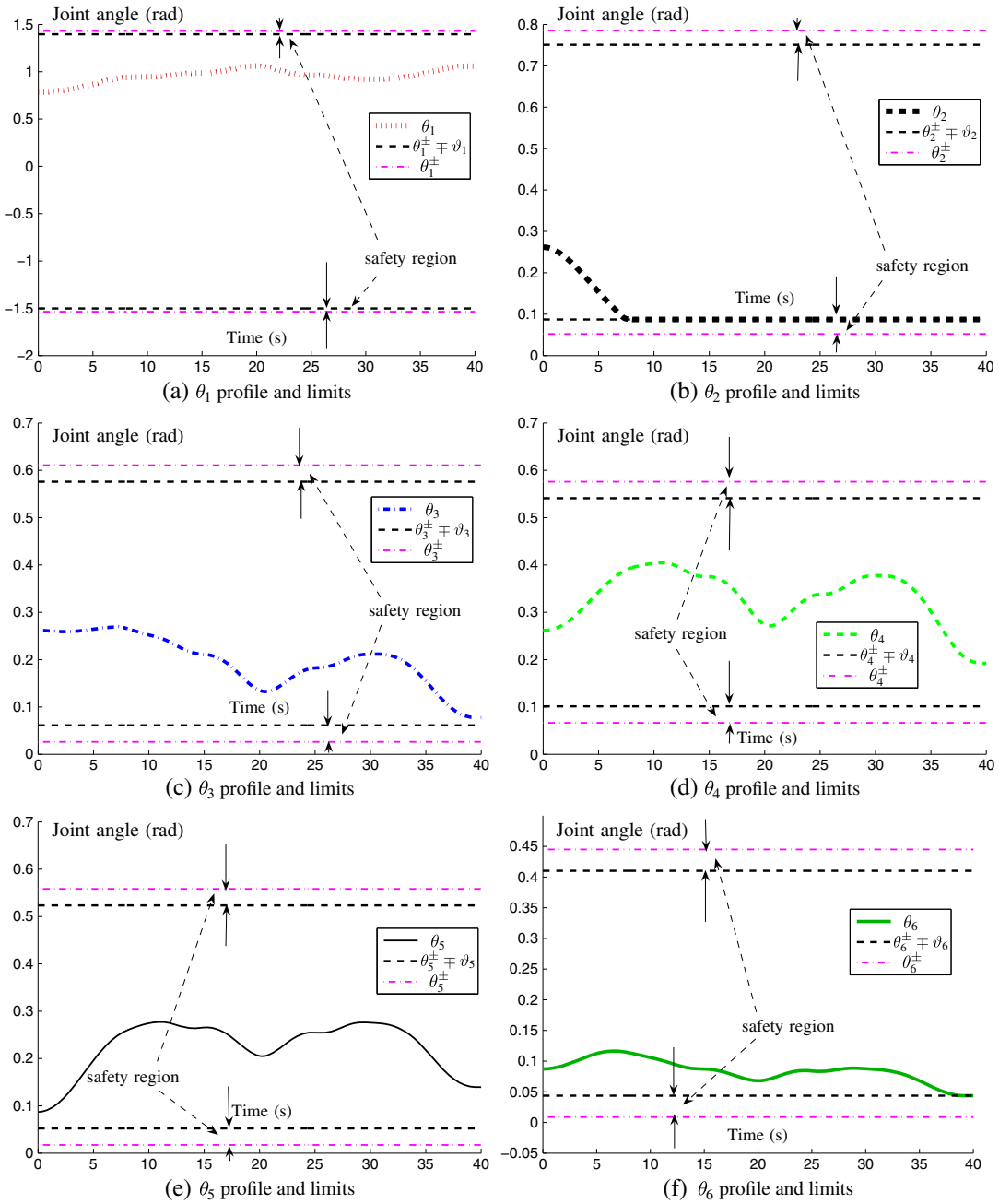

(a) θ_1 profile and limits (b) θ_2 profile and limits

(c) θ_3 profile and limits (d) θ_4 profile and limits

(e) θ_5 profile and limits (f) θ_6 profile and limits

Figure 6. Joint-angle profiles and corresponding limits of the planar 6-DOF manipulator tracking the "R" path synthesized by the TVCMM scheme with $p(t) = 2\sin(\pi t/T)$. (a) θ_1 profile and limits, (b) θ_2 profile and limits, (c) θ_3 profile and limits, (d) θ_4 profile and limits, (e) θ_5 profile and limits, and (f) θ_6 profile and limits.

DOI: 10.1002/oca

Following the two simulations (i.e., shown in Figures 3 and 4), we give Figure 5 which shows the comparative results about the profiles of manipulability index $w = \det(JJ^{\mathrm{T}})$ that are synthesized by the schemes with $p(t) = 2\sin(\pi t/T)$, $p(t) = 0$, and $p(t) = 1$. It can be seen from the figure that, when using the TVCMM scheme, the manipulability measure w is always larger compared to when using the scheme without a manipulability-maximizing index [i.e., with $p(t) = 0$]. That is to say,

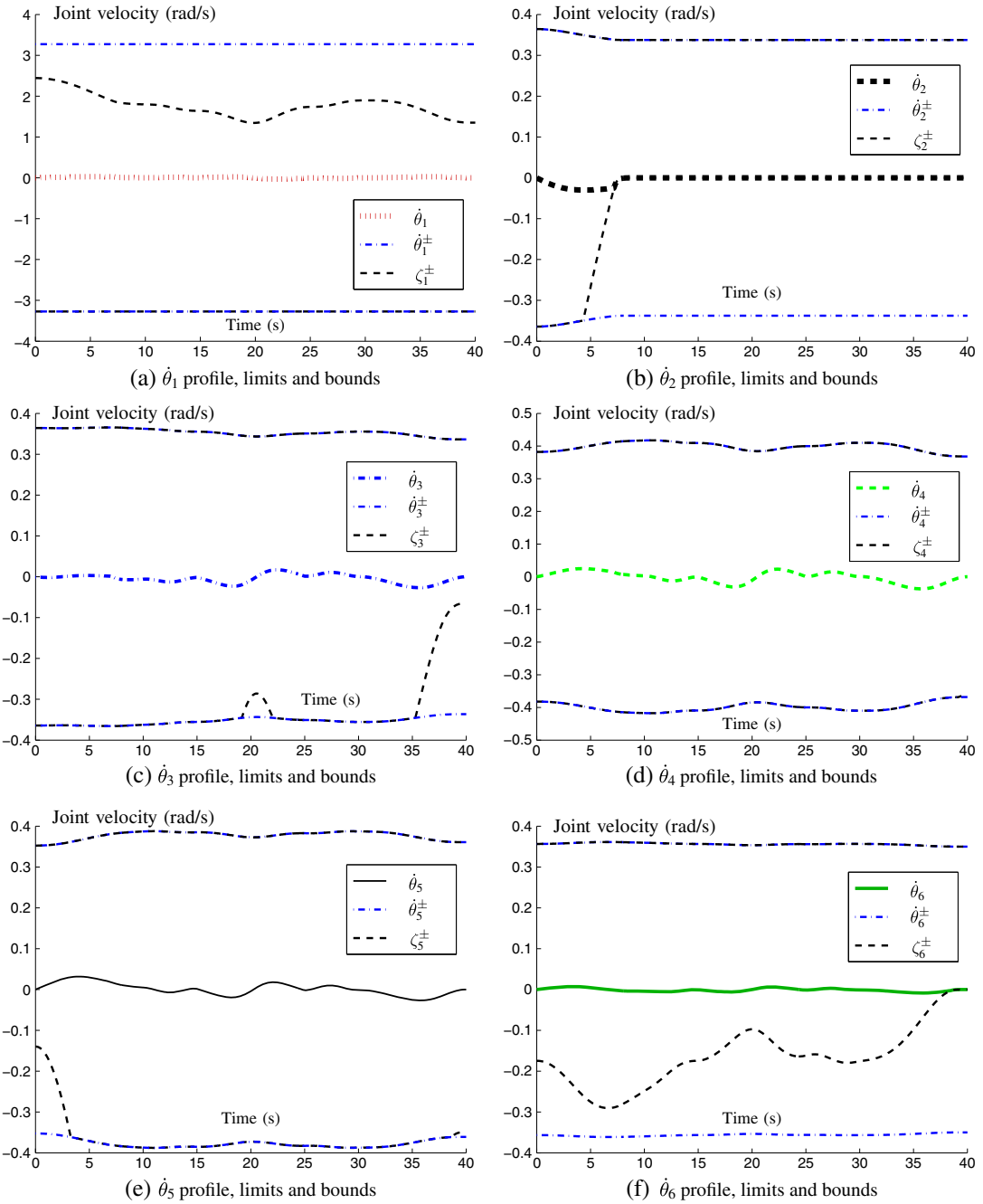

(a) $\dot{\theta}_1$ profile, limits and bounds

(b) $\dot{\theta}_2$ profile, limits and bounds

(c) $\dot{\theta}_3$ profile, limits and bounds

(d) $\dot{\theta}_4$ profile, limits and bounds

(e) $\dot{\theta}_5$ profile, limits and bounds

(f) $\dot{\theta}_6$ profile, limits and bounds

Figure 7. Joint-velocity profiles and corresponding limits and bounds of the planar 6-DOF manipulator tracking the "R" path synthesized by the TVCMM scheme with $p(t) = 2\sin(\pi t/T)$. (a) $\dot{\theta}_1$ profile, limits, and bounds; (b) $\dot{\theta}_2$ profile, limits, and bounds; (c) $\dot{\theta}_3$ profile, limits, and bounds; (d) $\dot{\theta}_4$ profile, limits, and bounds; (e) $\dot{\theta}_5$ profile, limits, and bounds; and (f) $\dot{\theta}_6$ profile, limits, and bounds.

DOI: 10.1002/oca

the manipulability of the manipulator is well improved, and the manipulator is farther away from singularities owing to the TVCMM scheme. It is worth mentioning that, when $p(t) = 0$, the scheme becomes an MVN scheme [26]. In addition, from the comparison between the profiles of manipulability measure w synthesized by the TVCMM scheme and the scheme with a constant coefficient [i.e., $p(t) = 1$], we can observe that the latter is a little larger than the former only at the beginning of the task duration, after which (from around $t = 8$ to $t = 40$ s), the w measures are nearly the same. Note that, as shown in Figure 3 and discussed in Section 3.1, the nonzero initial/final joint-velocity problem is caused by employing a constant coefficient [i.e., $p(t) = 1$], and that, by employing a time-varying coefficient [i.e., $p(t) = 2\sin(\pi t/T)$], the nonzero initial/final joint-velocity problem is remedied well. So, it can be concluded that the TVCMM scheme is a better choice for optimal motion planning and control of redundant robots, in view of its better performance in manipulability maximization and more suitability for engineering applications.

Furthermore, corresponding to the aforementioned simulation results synthesized by the TVCMM scheme with $p(t) = 2\sin(\pi t/T)$ (i.e., Figures 4 and 5), the joint angles and joint-angle limits are shown in more detail in Figure 6, which illustrates that all joint angles are kept within their physical limits. More specifically, none of the joint-angle profiles enter into the "safety region". In addition,

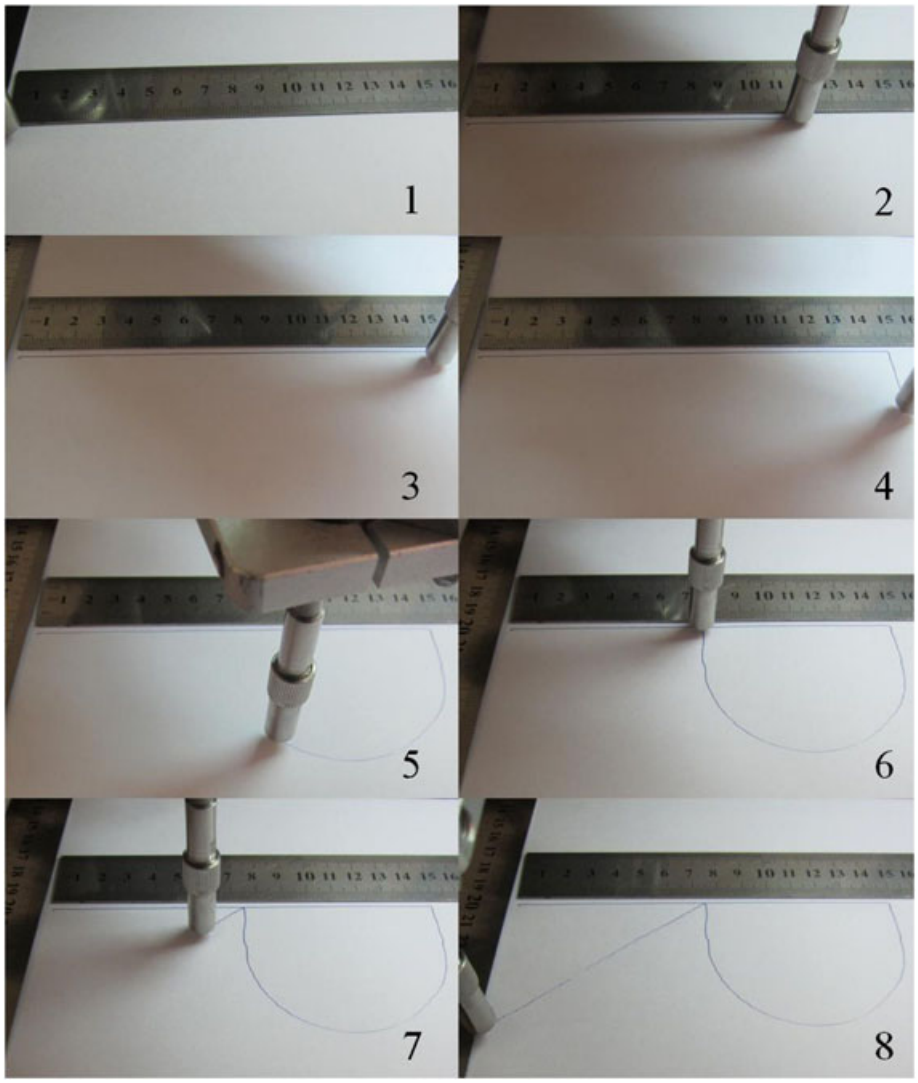

Figure 8. Snapshots for the actual end-effector task execution of the planar 6-DOF redundant robot manipulator tracking the "R" path synthesized by the TVCMM scheme with $p(t) = 2\sin(\pi t/T)$.

DOI: 10.1002/oca

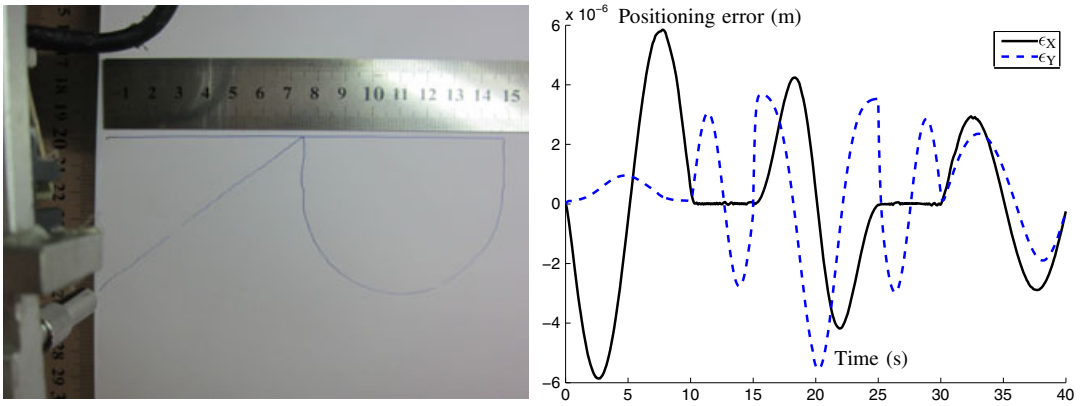

(a) Measurement of the "R" trajectory (b) Positioning error $\epsilon = r - f(\theta)$

Figure 9. The top-view measurement result of the "R" trajectory and the positioning error of the robot end-effector synthesized by the TVCMM scheme with $p(t) = 2\sin(\pi t/T)$. (a) Measurement of the "R" trajectory, (b) positioning error $\epsilon = r - f(\theta)$.

the joint velocities, the joint-velocity limits, and the combined bounds $\zeta_i^{\pm}$ are shown in Figure 7. It can be seen in Figure 7 that every joint-velocity $\dot{\theta}_i$ is within its physical limits, or more precisely, within the bounds $\zeta_i^{\pm}$, for $i = 1, 2, \cdots, 6$.

In summary, synthesized by the TVCMM scheme, the manipulability of the robot manipulator is increased without causing a nonzero initial/final joint-velocity problem, and the manipulator can also fulfill the end-effector task effectively (in addition to being farther away from singularities).

4.2. Experimental verification

Here, by using the TVCMM scheme, an experiment is performed on the planar 6-DOF push-rod-joint manipulator hardware system presented in Section 2. The task, the initial joint-angle state, and the parameters in the hardware experiment are set the same as before. The experimental results are illustrated in Figures 8 and 9. Specifically, Figure 8 shows the actual task execution of the manipulator synthesized by the TVCMM scheme subject to varying physical limits when the end-effector tracks the "R" path. This illustrates that the task is completed well. In addition, Figure 9 shows the top-view result of the "R" trajectory and the positioning errors. As seen from the figure, the height of letter "R" is nearly 0.15 m. As for the end-effector positioning errors, we can see in Figure 9(b) that the maximum positioning error is less than 6.0×10^{-6} m, which shows the high precision of the end-effector positioning synthesized by the proposed TVCMM scheme subject to varying limits.

In summary, this hardware experiment demonstrates well the physical realizability and efficacy of the proposed TVCMM scheme [which includes the numerical QP-solver (15)] subject to VJVL on the optimal motion planning and control of the planar 6-DOF redundant robot manipulator.

5. CONCLUSIONS

This paper designs and proposes a novel TVCMM scheme for the optimal control of redundant robot manipulators. The scheme is then reformulated into a unified QP problem which can be solved readily by the presented LVI-based numerical algorithm. Furthermore, the scheme is finally implemented on an actual planar 6-DOF robot manipulator. As illustrated via the simulations and the experiment performed on the 6-DOF manipulator, the manipulability of the robot can be maximized as compared with the MVN scheme. Besides, the proposed scheme can solve the nonzero initial/final joint-velocity problem. Moreover, the experimental results of tracking the "R" path demonstrate well the physical realization and efficacy of such a TVCMM scheme subject to varying physical limits. The end-effector positioning-error analysis validates, as well, the high precision of such a TVCMM scheme.

DOI: 10.1002/oca

ACKNOWLEDGEMENTS

This research was funded by the National Natural Science Foundation of China, with grant numbers 61075121 and 60935001, and by the Fundamental Research Funds for the Central Universities of China.

REFERENCES

1. Ji CY, Chen TC, Lee YL. Joint control for flexible-joint robot with input-estimation approach and LQG method. *Optimal Control Applications and Methods* 2008; **29**(2):101–125.
2. Vossen G, Maurer H. On L1-minimization in optimal control and applications to robotics. *Optimal Control Applications and Methods* 2006; **27**(6):301–321.
3. Khadem SE, Dubey RV. A global cartesian space obstacle avoidance scheme for redundant manipulators. *Optimal Control Applications and Methods* 1991; **12**(4):279–286.
4. Fabien BC. Direct optimization of dynamic systems described by differential-algebraic equations. *Optimal Control Applications and Methods* 2008; **29**(6):445–466.
5. Park DH, Hoffmann H, Pastor P, Schaal S. Movement reproduction and obstacle avoidance with dynamic movement primitives and potential fields. *IEEE-RAS International Conference on Humanoid Robots*, Daejeon, Korea, 2008; 91–98.
6. Zhang Y, Lv X, Li Z, Yang Z, Chen K. Repetitive motion planning of PA10 robot arm subject to joint physical limits and using LVI-based primal-dual neural network. *Mechatronics* 2008; **18**:475–485.
7. Komoguchi Y, Yano K, Peer A, Buss M. Redundancy resolution of a 7 DOF haptic interface considering collision and singularity avoidance. *IEEE/RSJ International Conference on Intelligent Robots and Systems*, Nice, France, 2008; 3513–3518.
8. Soylu S, Buckham BJ, Podhorodeski RP. Redundancy resolution for underwater mobile manipulators. *Ocean Engineering* 2010; **37**:325–343.
9. Mitsi S, Bouzakis KD, Sagris D, Mansour G. Determination of optimum robot base location considering discrete end-effector positions by means of hybrid genetic algorithm. *Robotics and Computer-Integrated Manufacturing* 2008; **24**:50–59.
10. Jun BH, Lee PM, Kim S. Manipulability analysis of underwater robotic arms on ROV and application to task-oriented joint configuration. *Journal of Mechanical Science and Technology* 2008; **22**:887–894.
11. Lee SH, Lee JH, Yi BJ, Kim SH, Kwak YK. Optimization and experimental verification for the antagonistic stiffness in redundantly actuated mechanisms: a five-bar example. *Mechatronics* 2005; **15**:213–238.
12. Zhang Y. Inverse-free computation for infinity-norm torque minimization of robot manipulators. *Mechatronics* 2006; **16**(3–4):177–184.
13. He B. A new method for a class of linear variational inequalities. *Mathematical Programming* 1994; **66**(1–3): 137–144.
14. Schreiber G, Otter M, Hirzinger G. Solving the singularity problem of non-redundant manipulators by constraint optimization. *Proceedings of International Conference on Intelligent Robots and Systems*, Kyongju, South Korea, 1999; **3**: 1482–1488.
15. Donelan PS. Singularities of robot manipulators. In *Singularity Theory*. World Scientific: Hackensack: NJ, USA, 2007; 189–217.
16. Yoshikawa T. Analysis and control of robot manipulators with redundancy. In *Robotics Research*, Brady M, Paul R (eds). MIT Press: Cambridge, MA, 1984; 735–747.
17. Huang J, Yamada D, Nakamura Y, Hara M, Yabuta T. Cooperative impedance control of a finger-arm robot by regulating finger's manipulability. *Journal of System Design and Dynamics* 2009; **3**(5):756–767.
18. Yoshikawa T. Manipulability of robotic mechanisms. *The International Journal of Robotics Research* 1985; **4**(2):3–9.
19. Kim JO, Khosla PK. Dexterity measures for design and control of manipulators. *Proceedings of IEEE/RSJ International Workshop on Intelligent Robots and Systems*, Osaka, Japan, 1991; **2**:758–763.
20. Tang CP, Krovi VN. Manipulability-based configuration evaluation of cooperative payload transport by mobile manipulator collectives. *Robotica* 2007; **25**:29–42.
21. Zhang Y, Chen K, Tan H. Performance analysis of gradient neural network exploited for online time-varying matrix inversion. *IEEE Transactions on Automatic Control* 2009; **54**(8):1940–1945.
22. Zhang Y, Ge SS. Design and analysis of a general recurrent neural network model for time-varying matrix inversion. *IEEE Transactions on Neural Networks* 2005; **16**(6):1477–1490.
23. Bazaraa M, Sherali H, Shetty C. *Nonlinear Programming: Theory and Algorithms*. John Wiley and Sons: Hoboken, New Jersey, 2006.
24. Siciliano B. Kinematic control of redundant robot manipulators: a tutorial. *Journal of Intelligent and Robotic Systems* 1990; **3**(3):201–212.
25. Nenchev DN. Tracking manipulator trajectories with ordinary singularities: a null space-based approach. *The International Journal of Robotics Research* 1995; **14**(4):399–404.
26. Zhang Y. Analysis and design of recurrent neural networks and their applications to control and robotic systems. *PhD Dissertation*, Chinese University of Hong Kong, 2002.

DOI: 10.1002/oca